

# Measured Impedance and Threshold Value of Electrode Line Impedance Supervision Based Protection in HVDC Transmission System

Qiang Sun, Bin Li, Jiawei He, and Ye Li

**Abstract**—At present, electrode line impedance supervision (ELIS) based protection is widely used to detect faults on grounding electrode lines, which are indispensable elements of high-voltage direct current (HVDC) systems. The existing theoretical analysis of measured impedance is based on lumped line model and the threshold value is generally set according to engineering experience, which have caused the dead zone problem and even accidents. Therefore, a study on measured impedance of ELIS-based protection and its threshold value selection method is carried out to solve this problem. In this study, the expressions of measured impedance under normal operation and fault conditions are deduced based on rigorous and accurate line model. Based on the expressions, the characteristics of the measured impedance are calculated and analyzed. With the characteristics of the measured impedance, the applicability of the protection with the traditional threshold value is further discussed and the distribution of the dead zone can be located. Then, the method to calculate the threshold value of ELIS-based protection is proposed. With a proper threshold value selected by the proposed method, the dead zone of ELIS-based protection is effectively eliminated, and the protection can identify all types of faults even with large transition resistances. Case studies on PSCAD/EMTDC have been conducted to verify the conclusion.

**Index Terms**—Grounding electrode line, electrode line impedance supervision (ELIS) based protection, measured impedance characteristic, threshold value selection.

## I. INTRODUCTION

HIGH-VOLTAGE direct current (HVDC) transmission systems represent an important revolution in power system owing to the advantages such as long transmission distance, low transmission loss, and narrow transmission corridor [1]–[4]. The grounding electrode is an indispensable part

of an HVDC system. Under the normal operation, the operation mode is bipolar. In this mode, the grounding electrode limits the voltage of converter neutral bus to be a reliable ground potential to ensure the symmetrical operation of the bipolar line. If either pole of the system is blocked due to faults or other reasons, the operation mode would be changed into the monopolar-ground mode [5]. In this mode, the transmission power will flow through the grounding electrode.

If the grounding electrode is installed in the converter station directly, the unbalanced current would directly flow into the ground in the converter station, leading to many problems. First, the DC current flowing into the ground may cause potential differences among substations at different locations. Therefore, the DC current flowing into the transformers may cause transformer saturation due to DC bias [6]–[8]. Besides, the DC current can also cause corrosion on the metal pipelines underground and affect the normal operation of the electrified railway [9], [10]. Consequently, the grounding electrode is usually located far from the converter station. As a result, for a grounding electrode line, it is necessary to connect the grounding electrode with the neutral bus of the converter station. To improve the operation reliability, the grounding electrode line is generally designed as double-circuit overhead lines on the same tower.

The protection of the grounding electrode line is essential to guarantee the reliability of the HVDC system. Generally, the conventional protection based on unbalanced current is applied in the monopolar-ground mode [11]. In the bipolar mode, the sensitivity of the conventional protection is not enough for various operation conditions. To solve this problem, ABB company designed a protection system based on signal injection, which is called grounding electrode line impedance supervision (ELIS) based protection [12]. By injecting high-frequency signal, the measured impedance can be used to detect the fault on the grounding electrode line. In recent years, some investigations have proposed novel strategies for ELIS-based protection, aiming to improve protection performance. Reference [13] proposes a frequency selection criterion to eliminate the protection dead zone. Reference [14] designs a novel protection criterion by introducing a voltage standing-wave ratio. It can avoid mis-operation under the condition of mismatching terminal resistors. Similar-

Manuscript received: January 17, 2022; revised: April 15, 2022; accepted: August 18, 2022. Date of CrossCheck: August 18, 2022. Date of online publication: September 28, 2022.

This work was supported by the National Natural Science Foundation of China for Distinguished Young Scholars (No. 52025071) and the Joint Funds of the National Natural Science Foundation of China (No. U1866205).

This article is distributed under the terms of the Creative Commons Attribution 4.0 International License (<http://creativecommons.org/licenses/by/4.0/>).

Q. Sun, B. Li (corresponding author), and J. He are with the Key Laboratory of Smart Grid of Ministry of Education, Tianjin University, Tianjin, China (e-mail: sunqtj@163.com; binli@tju.edu.cn; hejiawei\_tju@126.com).

Y. Li is with the State Key Laboratory of Reliability and Intelligence of Electrical Equipment, Hebei University of Technology, Tianjin, China (e-mail: liye@hebut.edu.cn).

DOI: 10.35833/MPCE.2022.000035



ly, the transverse difference ratio of head-end high-frequency measured impedance and voltage amplitude integration are also used in the protection scheme in [15] and [16]. By injecting two frequency signals, [17] proposes an improved protection scheme to eliminate the dead zones. Reference [18] analyzes the performance of ELIS-based protection under different types of line break faults. The results show that the protection will not identify single-line break fault under the condition that the grounding electrode line length is integer multiple of the half wavelength of the injected signal.

An accurate measured impedance is the basis of designing the ELIS-based protection scheme. The previous investigations on measured impedance of ELIS-based protection are generally based on lumped parameters of the line and not accurate enough. Reference [13] uses  $\pi$  model of the line to analyze the impedance characteristic although the grounding electrode line length is several times of the wavelength. Reference [14] omits the coupling effect of the double-circuit lines. It leads to an inaccurate measured impedance under different kinds of faults. Therefore, it is necessary for the protection of grounding electrode line to obtain the accurate calculation method of the measured impedance. Besides, the threshold value of the existing ELIS-based protection is generally set to be  $30 \Omega$  according to the experience judgment [14]. Without reasonable threshold value, the protection of grounding electrode line cannot accurately identify faults based on measured impedance.

As discussed above, the inaccurate measured impedance and the improper threshold value lead to the dead zone of the protection for grounding electrode lines. If a fault occurs on the grounding electrode line and is not detected in bipolar mode, the HVDC system cannot be switched from bipolar mode into monopolar-ground mode when necessary. This is because a fault on the grounding electrode line during monopolar-ground mode may also produce a fire because the fault current can reach the level of 5 A to 10 A [19]. Consequently, the whole HVDC system must be stopped and would result in huge power loss. The actual fault accident shows that there is dead zone for the existing ELIS-based protection. In June 2014, a fault occurred on the grounding electrode line in an HVDC project in southwest China and the protection did not detect the fault correctly [20]. Therefore, locating and eliminating the dead zone of the protection of grounding electrode line is essential for the operation security and reliability of the HVDC system.

In this study, the accurate analysis of the fault on grounding electrode line is firstly studied, which lays the basis for the design of a reasonable protection scheme and the improvement of the protection sensitivity. Then, based on the calculation method and the property of the measured impedance, the dead zone existing in ELIS-based protection is located, and it is concluded that the dead zone is caused by the improper threshold value selection. Based on that, a threshold value selection method is proposed instead of the empirical value leading to dead zone, and the selection method can completely eliminate the dead zone and improve the security and reliability of the HVDC system. In sum, this paper is organized as follows. In Section II, the sinusoidal

steady-state equation of electromagnetic wave process is used to calculate the measured impedance under normal operation. In Section III, the measured impedance under different faults is further calculated, and the operation characteristics of the protection are analyzed. On this basis, a criterion for threshold value selection is given to eliminate the dead zone of ELIS-based protection, to detect fault with high transition resistance. The correctness of theoretical analysis and effectiveness of threshold value selection criterion are verified on PSCAD/EMTDC in Section IV. Finally, the conclusions are given in Section V.

## II. ELIS-BASED PROTECTION AND MEASURED IMPEDANCE UNDER NORMAL OPERATION

The measured impedance is the core of ELIS-based protection. To analyze the applicability of the threshold value and propose the threshold value selection method, the characteristics of measured impedance are investigated. Therefore, the accurate measured impedance expressions should be first deduced, which is the basis for analyzing measured impedance. In this section, the ELIS-based protection is introduced, and then the expression of measured impedance under normal operation is deduced, as a case for establishing the derivation method of measured impedance expressions.

### A. Grounding Electrode Line and Fault Detection

In the HVDC transmission system, the power converter station is used to realize the power conversion and its basic topology is shown in Fig. 1(a). Under the normal operation, the DC current circulates in the positive and negative pole lines. Thus, no current flows into the ground through the grounding electrode. When the system operates in unbalanced state, the thousand-ampere DC current flows into the ground through the grounding electrode. To avoid the negative influence of the DC current, the grounding electrode is usually installed far from the power converter station [20], and the grounding electrode line is developed to connect the neutral bus of the converter station and grounding electrode, whose typical structure and geometric parameters are shown in Fig. 1(b) and (c), respectively. In Fig. 1(c), the relative  $x$ -position of tower center is 0 m, which indicates that the tower is centered, the height of the grounding electrode lines is 31 m, the horizontal spacing between the grounding electrode lines is 6 m, while the height of overhead grounding wire over the grounding electrode lines is 6 m. Each grounding electrode line has two sub-conductors and their spacing is 0.4 m. Besides, the sags of the grounding electrode lines and the overhead grounding wire are 15 m and 12 m, respectively, which are the differences between the tower height and the mid-span height.

In the existing HVDC projects, the measurement instruments and communication devices are generally not installed at the grounding electrode side because it is far from the power converter station and the power supply for the devices is difficult. Therefore, only the currents and voltages at the converter station side are measured. To inject the high-frequency signal to the grounding electrode line, a current source is installed at the terminal of grounding electrode line

close to the converter station, as shown in Fig. 1(b). Specifically, the current signal on the grounding electrode line is measured and compared with the default value, and the waveform parameters of the target current signal are calculated by proportional-integral (PI) control. Then, according to the parameters, the target current signal can be generated by

the digital sinusoidal oscillator, which can be easily programmed with digital signal processing (DSP). Finally, the generated current signal is amplified and injected to the grounding electrode line [16]. The whole structure has negative feedback to stabilize the injected current.

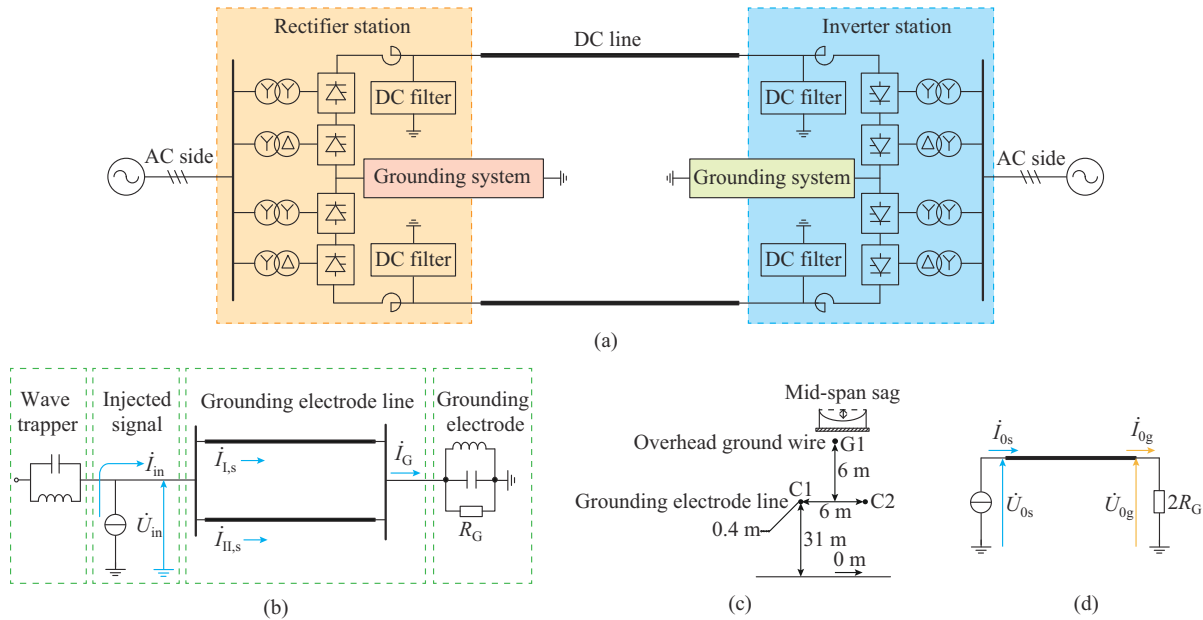


Fig. 1. Structure of HVDC system with grounding electrode line. (a) Basic topology of HVDC transmission system. (b) Structure of grounding electrode line. (c) Geometric parameter of grounding electrode line. (d) Ground-mode network under normal operation.

With the current injection, the voltage and current at the line terminal are measured to calculate the measured impedance. If a fault occurs, the impedance varies correspondingly, which is significantly different from that under normal operation. According to this characteristic, the impedance protection can detect the fault [13].

In addition, a wave trapper is installed to prevent the injected current from flowing into the station. In general, the wave trapper is composed of the inductor and capacitor in parallel, which form a parallel resonance at the frequency of injected signal. The inductor can also serve as a path for the DC current. Besides, a matched resistor is at the electrode side, whose function is to reduce the standing wave effect on the grounding electrode line. To provide a DC current path, an inductor is parallel with the matched resistance, while a capacitor is also parallel to keep the whole impedance matched.

At the protection position, the measured impedance  $Z_{\text{mea}}$  is defined as:

$$Z_{\text{mea}} = \frac{\dot{U}_{\text{in}}}{\dot{I}_{\text{in}}} \quad (1)$$

where  $\dot{I}_{\text{in}}$  is the injected current; and  $\dot{U}_{\text{in}}$  is the measured voltage. The fault detection criterion is designed as [14]:

$$|Z_{\text{mea}} - Z_{\text{normal}}| < Z_{\text{set}} \quad (2)$$

where  $Z_{\text{normal}}$  is the measured impedance under normal operation; and  $Z_{\text{set}}$  is the threshold value. Compared with normal conditions, the measured impedance changes after faults and (2) is not valid. Therefore, the fault can be detected accord-

ing to the criterion. It should be noted that, because the ELIS-based protection is designed for grounding electrode lines and has nothing to do with the system structure, it is applicable to both line-commutated converter based HVDC (LCC-HVDC) systems and voltage source converter based HVDC (VSC-HVDC) systems that include grounding electrode lines.

### B. Analysis of Measured Impedance Under Normal Operation

In this subsection, the calculation expression of the measured impedance under normal operation is first deduced. The grounding electrode line can be equivalent to distributed parameter circuit. The sinusoidal steady-state equation of the electromagnetic wave process propagating on the grounding electrode line is shown as [21], [22]:

$$\begin{cases} \dot{U}_{L2} = \dot{U}_{L1} \cosh(\gamma l_{12}) - \dot{I}_{L1} Z_c \sinh(\gamma l_{12}) \\ \dot{I}_{L2} = \dot{I}_{L1} \cosh(\gamma l_{12}) - \frac{\dot{U}_{L1}}{Z_c} \sinh(\gamma l_{12}) \end{cases} \quad (3)$$

where  $\gamma$  and  $Z_c$  are the propagation coefficient and wave impedance, respectively;  $\dot{U}_{L1}$ ,  $\dot{U}_{L2}$  and  $\dot{I}_{L1}$ ,  $\dot{I}_{L2}$  are the voltages and currents at two points, respectively; and  $l_{12}$  is the distance between the two points.

In practical HVDC systems, the grounding electrode lines are generally double-circuit. Therefore, the decoupling concept used for the DC transmission line (positive and negative pole lines) is also applicable for the coupling effect between double-circuit lines of the grounding electrode line

[23], [24]. After decoupling, (3) is satisfied both in the line-mode and ground-mode networks.

Figure 1(b) shows the equivalent circuit of the grounding electrode line under normal operation, where the double lines are marked as line I and line II to distinguish them from each other, respectively. Correspondingly,  $\dot{I}_{1s}$  and  $\dot{I}_{1l}$  are the currents on line I and line II at the station side, respectively. Besides,  $\dot{I}_G$  is defined as the current flowing into the ground through the grounding electrode; and  $R_G$  is the matched resistance, whose value is generally selected as half of the ground-mode wave impedance. As the wave trapper can prevent the current from flowing into the converter station, the wave trapper and station do not need to be considered in the analysis. Similarly, the impedance of the parallel structure at the grounding electrode for the injected signal is equal to  $R_G$ , so the inductor and capacitor do not need to be considered in the analysis either.

According to Fig. 1(b), the ground-mode voltage at the station side  $\dot{U}_{0s}$  can be calculated as  $\sqrt{2}\dot{U}_{in}$ , and the ground-mode current at the station side  $\dot{I}_{0s}$  can be calculated as  $\sqrt{2}\dot{I}_{in}/2$ . Similarly, the ground-mode voltage and current at the grounding electrode side can be calculated as  $\dot{U}_{0g} = \sqrt{2}\dot{I}_G R_G$  and  $\dot{I}_{0g} = \sqrt{2}\dot{I}_G/2$ , respectively. The ground-mode network and the corresponding variables are shown in Fig. 1(d). Moreover, the line-mode voltages and currents are all zero because the double-circuit line is symmetrical under normal operation.

Then, the relationship among  $\dot{I}_G$ ,  $\dot{U}_{in}$ , and  $\dot{I}_{in}$  can be obtained as:

$$\begin{cases} \sqrt{2}\dot{I}_G R_G = \sqrt{2}\dot{U}_{in} \cosh(\gamma_0 l) - \frac{\sqrt{2}}{2}\dot{I}_{in} Z_{c0} \sinh(\gamma_0 l) \\ \frac{\sqrt{2}}{2}\dot{I}_G = \frac{\sqrt{2}}{2}\dot{I}_{in} \cosh(\gamma_0 l) - \frac{\sqrt{2}\dot{U}_{in}}{Z_{c0}} \sinh(\gamma_0 l) \end{cases} \quad (4)$$

where  $l$  is the length of the line;  $\gamma_0$  is the ground-mode propagation coefficient; and  $Z_{c0}$  is the ground-mode wave impedance, which can be calculated according to [25].

According to (4), the measured impedance defined by (1) can be calculated as:

$$Z_{\text{normal}} = \frac{\dot{U}_{in}}{\dot{I}_{in}} = \frac{1}{2} Z_{c0} \frac{Z_{c0} \sinh(\gamma_0 l) + 2R_G \cosh(\gamma_0 l)}{Z_{c0} \cosh(\gamma_0 l) + 2R_G \sinh(\gamma_0 l)} \quad (5)$$

In general, the matched resistance  $R_G = Z_{c0}/2$  and the measured impedance under normal operation can be further simplified as  $Z_{\text{normal}} = Z_{c0}/2$ .

In this section, the ELIS-based protection is introduced, and the derivation method of measured impedance expressions is proposed, which is based on the electromagnetic wave theory and decoupling concept. And the measured impedance under normal operation is deduced. With the derivation method, the expressions under fault conditions can also be deduced and the difference between measured impedances under normal operation and under faults can be discussed.

### III. ANALYSIS OF MEASURED IMPEDANCE UNDER FAULT CONDITIONS AND THRESHOLD VALUE SELECTION METHOD

The measured voltage  $\dot{U}_{in}$  will change when a fault oc-

curr. As the injected current is constant, the measured impedance changes with the voltage. The protection of the grounding electrode line mainly uses the difference of measured impedance to detect the fault. Therefore, the expressions of measured impedance under fault conditions are deduced with the method based on the electromagnetic wave theory and decoupling concept in this section. Then, with the expressions, the characteristics of the measured impedance under faults can be easily obtained, and the applicability of the empirical threshold value is discussed. Due to the limitation of empirical value in detecting faults with high transition resistance, a threshold value selection method is proposed to solve the problem and avoid the harm of faults with high transition resistance, such as power loss and fire risk.

#### A. Measured Impedance Under Fault Conditions

Two types of faults are identified on the grounding electrode line, i.e., double line-to-ground fault and single line-to-ground fault. Figure 2(a) shows the equivalent circuit of a double line-to-ground fault occurring on the grounding electrode line. In Fig. 2, various types of faults are represented by different transition resistance values, where  $R_1$  and  $R_2$  are the transition resistances between the lines; and  $R_3$  is the transition resistance between the line and the ground. Figure 2(a) can be decoupled into a ground-mode network and a line-mode network, as shown in Fig. 2(b) and (c), respectively, according to the decoupling transform theory. The double line-to-ground fault is first analyzed, where transition resistance exists between the lines, i.e.,  $R_1 = R_2 \neq 0$ . Considering that the network remains symmetrical after double line-to-ground fault, the line-mode voltages and currents are all zero, which is similar to the normal operation condition.

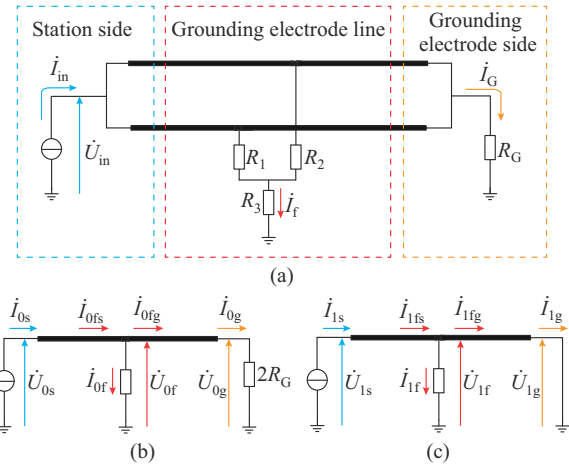


Fig. 2. Grounding electrode line with double line-to-ground fault. (a) Equivalent circuit. (b) Ground-mode network. (c) Line-mode network.

The ground-mode voltages  $\dot{U}_{0s}$  and  $\dot{U}_{0g}$  and currents  $\dot{I}_{0s}$  and  $\dot{I}_{0g}$  are still the same as those in (4). The ground-mode current and voltage at the fault point, i.e.,  $\dot{I}_{0f}$  and  $\dot{U}_{0f}$ , can be calculated as:

$$\begin{cases} \dot{I}_{0f} = \frac{\sqrt{2}}{2} \dot{I}_f \\ \dot{U}_{0f} = \frac{\sqrt{2}}{2} \dot{I}_f (R_1 + 2R_3) = \frac{\sqrt{2}}{2} \dot{I}_f R_{eq} \end{cases} \quad (6)$$

where  $\dot{I}_f$  is the fault current.

After decoupling, the line segments from the fault to the two terminals still satisfy (3). As the line is divided into two parts by the fault point, the ground-mode currents at both sides of the fault, i.e.,  $\dot{I}_{0fs}$  and  $\dot{I}_{0fg}$ , are also necessary for the analysis. For the segment between the fault point and the grounding electrode,  $\dot{U}_{of}$  and  $\dot{I}_{0fg}$  can be calculated from  $\dot{U}_{0g}$  and  $\dot{I}_{0g}$  according to (3), i.e.,

$$\begin{cases} \dot{U}_{of} = \dot{U}_{0g} \cosh(\gamma_0(l-x)) + \dot{I}_{0g} Z_{c0} \sinh(\gamma_0(l-x)) \\ \dot{I}_{0fg} = \dot{I}_{0g} \cosh(\gamma_0(l-x)) + \frac{\dot{U}_{0g}}{Z_{c0}} \sinh(\gamma_0(l-x)) \end{cases} \quad (7)$$

where  $x$  is the fault distance from the station side. For the segment between the fault point and the station,  $\dot{U}_{of}$  and the ground-mode current at the left side of the fault point  $\dot{I}_{0fs}$  can be calculated from  $\dot{I}_{0s}$  and  $\dot{U}_{0s}$  according to (3).

According to (6) and (7), the fault current  $\dot{I}_f$  can be expressed as:

$$\dot{I}_f = \dot{I}_G \frac{Z_{c0}}{R_{eq}} (\cosh(\gamma_0(l-x)) + \sinh(\gamma_0(l-x))) \quad (8)$$

Then, due to  $\dot{I}_{0fs} = \dot{I}_{0fg} + \dot{I}_{of}$ ,  $\dot{I}_{0fs}$  can be expressed as:

$$\dot{I}_{0fs} = \frac{\sqrt{2}}{2} \dot{I}_G \left[ \cosh(\gamma_0(l-x)) + \sinh(\gamma_0(l-x)) + \frac{Z_{c0}}{R_{eq}} (\cosh(\gamma_0(l-x)) + \sinh(\gamma_0(l-x))) \right] \quad (9)$$

Because  $\dot{I}_{0fs}$  can be calculated from both terminals of the line, the other expressions can be obtained. According to the two expressions, the relationship between the ground current  $\dot{I}_G$  and injected current  $\dot{I}_{in}$  can be expressed as:

$$\dot{I}_G = \dot{I}_{in} \left[ \cosh(\gamma_0 l) + \sinh(\gamma_0 l) + \frac{Z_{c0}}{R_{eq}} (\cosh(\gamma_0(l-x)) + \sinh(\gamma_0(l-x))) \cosh(\gamma_0 x) \right] \quad (10)$$

In addition,  $\dot{U}_{0s}$  can be calculated as:

$$\dot{U}_{0s} = \dot{U}_{of} \cosh(\gamma_0 x) + \dot{I}_{0fs} Z_{c0} \sinh(\gamma_0 x) \quad (11)$$

Furthermore,  $\dot{U}_{in}$  can be obtained by combining (8)-(11). Then, under the double line-to-ground fault, the measured impedance  $Z_{mea,dou}$  is calculated as:

$$Z_{mea,dou} = \frac{1}{2} Z_{c0} \frac{\sinh(\gamma_0 l) + \cosh(\gamma_0 l) + \frac{Z_{c0} \sinh(\gamma_0 x)}{R_{eq}} g(x)}{\sinh(\gamma_0 l) + \cosh(\gamma_0 l) + \frac{Z_{c0} \cosh(\gamma_0 x)}{R_{eq}} g(x)} \quad (12)$$

where  $g(x) = \sinh(\gamma_0(l-x)) + \cosh(\gamma_0(l-x))$ .

However, (12) is not suitable for metallic faults. Therefore, the measured impedance under metallic double line-to-ground fault is also analyzed. When a metallic fault occurs, the ground-mode voltage at the fault point can be expressed as:

$$\dot{U}_{of} = 0 = \dot{U}_{0s} \cosh(\gamma x) - \dot{I}_{0s} Z_{c0} \sinh(\gamma x) \quad (13)$$

The measured impedance under metallic double line-to-ground fault is calculated as:

$$Z_{mea,dou} = \frac{1}{2} Z_{c0} \tanh(\gamma_0 x) \quad (14)$$

According to (12) and (14), it can be found that the measured impedance under the double line-to-ground fault is affected by the fault distance and transition resistance, which is significantly different from the measured impedance under normal operation shown in (5).

When a single line-to-ground fault occurs ( $R_1 = 0$  and  $R_2 = \infty$ ), the line-mode and ground-mode networks can also be obtained from decoupling. However, the single line-to-ground fault is not symmetrical so the line-mode voltages and currents are not zero. Therefore, the line-mode voltages and currents need to be analyzed separately, and a similar method as above is still feasible. Due to space limitations, the specific derivation is omitted in this paper.

Under the single line-to-ground fault, the measured impedance  $Z_{mea,sin}$  is deduced as:

$$Z_{mea,sin} = \frac{1}{2} Z_{c0} \frac{\sinh(\gamma_0 l) + \cosh(\gamma_0 l) + \frac{Z_{c0} \sinh(\gamma_0 x)}{R_{eq} + f(x)} g(x)}{\sinh(\gamma_0 l) + \cosh(\gamma_0 l) + \frac{Z_{c0} \cosh(\gamma_0 x)}{R_{eq} + f(x)} g(x)} \quad (15)$$

where  $f(x) = (\sinh(\gamma_1(l-x))\sinh(\gamma_1 x)/\sinh(\gamma_1 l))Z_{c1}$ ;  $R_{eq} = 2R_3$  because no transition resistance exists between the lines under the single line-to-ground fault;  $\gamma_1$  is the line-mode propagation coefficient; and  $Z_{c1}$  is the line-mode wave impedance, which can also be calculated according to [24]. Equation (15) is suitable for metallic faults.

When a single line-to-ground fault occurs, it can be observed that the measured impedance is also different from that under normal operation. Equations (5), (12), (14), and (15) indicate that the measured impedance under the double line-to-ground fault or single line-to-ground fault varies from that under normal operation, which provides the theoretical basis for the impedance protection of the grounding electrode line. However, in practical engineering, the selection of the threshold value  $Z_{set}$  is still very rough. For example, in [14], it is selected as 30  $\Omega$ , which is an empirical value. In addition, an inappropriate threshold value reduces the operation sensitivity of the impedance protection. Therefore, the effective method to select the threshold value for the impedance protection needs to be studied.

### B. Characteristics of Measured Impedance

With the preceding derivation, the detailed characteristics of the measured impedance can be analyzed. As an example, a metallic double line-to-ground fault is first discussed. In practical engineering, the length of the grounding electrode line is generally at the level of hundreds of kilometers, so here, the line length 100 km is used as an example. When the fault distance changes from 0 km to 100 km in the system shown in Fig. 1(a), the measured impedance can be calculated according to (15). The calculation result is presented in Fig. 3.

As shown in Fig. 3, the trajectory of the measured impedance  $Z_{mea}(l)$  is spiral, whose center is the measured impedance under normal operation  $Z_{normal}$ . Furthermore, the operation boundary of the protection is a circle whose center is al-

so the measured impedance under normal operation  $Z_{\text{normal}}$  and radius is the threshold value  $Z_{\text{set}}$ . In the existing engineering project,  $Z_{\text{set}}$  is generally selected as an empirical value  $30 \Omega$ . Obviously, when  $x=l$ , the measured impedance  $Z_{\text{mea}}(l)$  is the closest to the measured impedance  $Z_{\text{normal}}$  under normal operation. Therefore,  $Z_{\text{set}}$  should be larger than  $|Z_{\text{mea}}(l) - Z_{\text{normal}}|$  to identify the normal operation condition and fault condition. As shown in Fig. 3,  $|Z_{\text{mea}}(l) - Z_{\text{normal}}| = 53.18 \Omega$ , which is larger than  $Z_{\text{set}}$  and it means that the protection with the empirical threshold value can effectively distinguish the normal operation condition and metallic fault condition (the same conclusion can be found for a single line-to-ground fault condition).

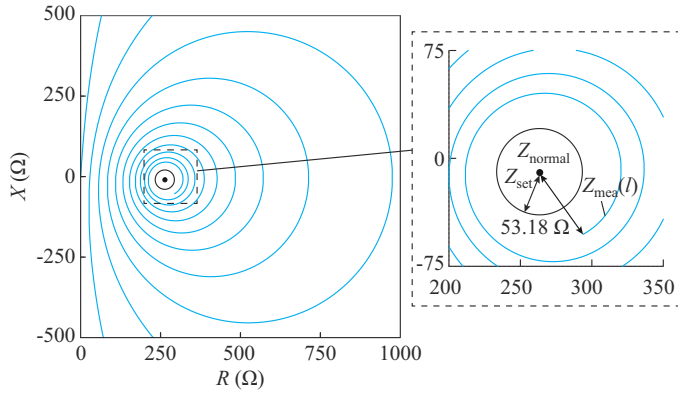


Fig. 3. Trajectory of measured impedance under metallic double line-to-ground fault.

However, in practical engineering, the transition resistance may exist in faults. Therefore, its influence should be considered. When  $R_3$  changes from  $0 \Omega$  to  $300 \Omega$  and  $x$  changes from  $0 \text{ km}$  to  $100 \text{ km}$ , the measured impedance is calculated, and the trajectories is shown in Fig. 4.

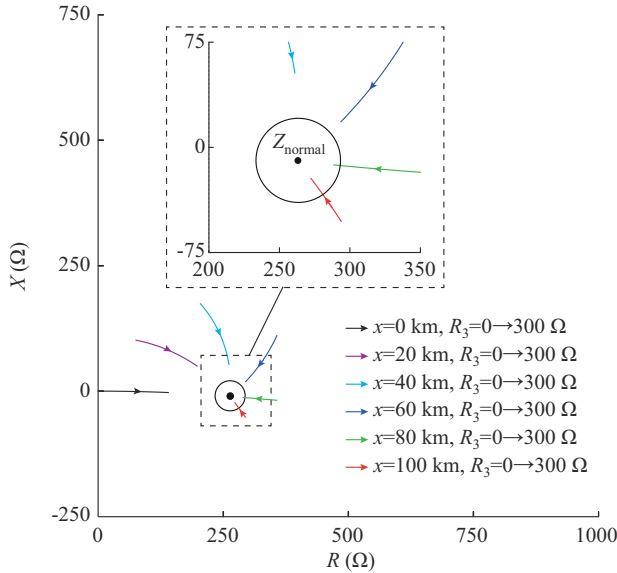


Fig. 4. Trajectories of measured impedance under double line-to-ground fault when  $R_3$  and  $x$  change.

In Fig. 4, each trajectory represents the change of measured impedance with  $R_3$  under a certain fault distance  $x$ , i.e.,

$x = 0, 20, \dots, 100 \text{ km}$ . The trajectories are marked in green and red when part of the trajectory comes into the operation boundary circle under this fault distance. For example, when  $x = 100 \text{ km}$ , the measured impedance is in the operation boundary circle when  $R_3 = 95.8 \Omega$ , i.e.,  $R_{\text{eq}} = 191.6 \Omega$ . This means that the protection cannot identify the fault under this condition. Therefore, with the empirical threshold value, the capability against transition resistance of the impedance protection is reduced substantially. However, as mentioned in Section I, a fault with high transition resistance caused by a branch is more likely to occur on grounding electrode lines, which usually pass through mountains, and the fault with high transition resistance is very likely to cause fire. Therefore, the threshold value selection should be more accurate to improve the protection operation sensitivity.

### C. Improved Threshold Value Selection Method

According to the previous analysis, the larger the fault distance is, and the larger the transition resistance is, the closer the fault measured impedance to the normal operation measured impedance will be. Therefore, the threshold value should satisfy  $Z_{\text{set}} < |Z_{\text{mea}}(l, R_{\text{eq,max}}) - Z_{\text{normal}}|$ .

When  $x = l$ , we can obtain:

$$\begin{cases} f(l, R_{\text{eq,max}}) = \frac{\sinh(\gamma_1(l-l))\sinh(\gamma_1 l)}{\sinh(\gamma_1 l)} \frac{Z_{c1}}{R_{\text{eq,max}}} + 1 = 1 \\ g(l) = \sinh(\gamma_0(l-l)) + \cosh(\gamma_0(l-l)) = 1 \end{cases} \quad (16)$$

When  $f(l, R_{\text{eq,max}}) = 1$  and  $g(l) = 1$ , according to (12) and (15), it can be obtained that  $Z_{\text{mea,dou}} = Z_{\text{mea,sin}}$ . In this manner, the measured impedances under the single line-to-ground fault and double line-to-ground fault when  $x = l$  and  $R_{\text{eq}} = R_{\text{eq,max}}$  are the same, i.e.,

$$Z_{\text{mea}}(l, R_{\text{eq,max}}) = \frac{1}{2} Z_{c0} \frac{\sinh(\gamma_0 l) + \cosh(\gamma_0 l) + \frac{Z_{c0}}{R_{\text{eq,max}}} \sinh(\gamma_0 l)}{\sinh(\gamma_0 l) + \cosh(\gamma_0 l) + \frac{Z_{c0}}{R_{\text{eq,max}}} \cosh(\gamma_0 l)} \quad (17)$$

Therefore, the upper limit of the threshold value can be calculated as:

$$Z_{\text{set,up}} = |Z_{\text{mea}}(l, R_{\text{eq,max}}) - Z_{\text{normal}}| = \frac{1}{2} \frac{Z_{c0}^2}{R_{\text{eq}}} \cdot \left| \frac{1}{\sinh(\gamma_0 l) + \cosh(\gamma_0 l)} \frac{1}{\sinh(\gamma_0 l) + \cosh(\gamma_0 l) + \frac{Z_{c0}}{R_{\text{eq}}} \cosh(\gamma_0 l)} \right| \quad (18)$$

The threshold value of the protection should be smaller than  $Z_{\text{set,up}}$  to guarantee the protection operation sensitivity. According to the proposed method and line parameters calculated from the line structure shown in Fig. 1(c),  $Z_{\text{set,up}}$  is calculated as  $15.52 \Omega$ .

However, in practical engineering, it is impossible to calculate the line parameters completely accurately, which means that the calculation error must exist. Therefore, the effect of line parameter calculation error should be analyzed.

Here, the influence of the line ground-mode wave impedance  $Z_{c0}$  with different calculation errors is mainly discussed. Figure 5 shows the calculated impedance according to (12) under double line-to-ground with transition resistance of  $300\ \Omega$  when the calculated wave impedance  $Z_{c0}$  has errors of  $-3\%$  and  $3\%$ . As shown in Fig. 5(a), when  $Z_{c0}$  has an error of  $-3\%$ , both the measured impedances under normal operation ( $Z_{-E}$  indicated by the red point) and fault condition (the red spiral trajectory) shift. However, the shifting range and direction under the normal operation and fault conditions are almost the same. This makes the distance between  $Z_{\text{normal}}$  and  $Z_{\text{mea}}(l, R_{\text{eq,max}})$  almost unchanged. As shown in Fig. 5(a), the value of  $|Z_{\text{mea}}(l, R_{\text{eq,max}}) - Z_{-E}|$  is  $15.09\ \Omega$  when  $Z_{c0}$  has an error of  $-3\%$ , which is very close to the value  $15.52\ \Omega$  under the condition without error. Similarly, as shown in Fig. 5(b), when  $Z_{c0}$  has an error of  $3\%$ , the calculated impedances under normal operation  $Z_{+E}$  and fault conditions shift with the same direction and a similar range.  $|Z_{\text{mea}}(l, R_{\text{eq,max}}) - Z_{+E}|$  is  $15.94\ \Omega$ , which is also very close to  $15.52\ \Omega$ . That is, although the measured impedance changes when the error of  $Z_{c0}$  is considered, the value of  $|Z_{\text{mea}}(l, R_{\text{eq,max}}) - Z_{\text{normal}}|$  is almost unchanged. Thus, it can be concluded that the calculation error of wave impedance does not affect the calculation of the upper limit of the threshold value  $Z_{\text{set,up}}$ .

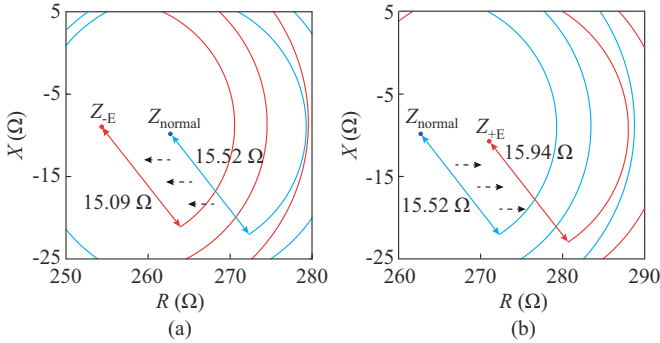


Fig. 5. Positions of calculated impedance. (a) With an error of  $-3\%$ . (b) With an error of  $3\%$ .

Therefore, the threshold value is set as:

$$Z_{\text{set}} = Z_{\text{set,up}} / K_{\text{sen}} \quad (19)$$

where  $K_{\text{sen}}$  is the sensitivity coefficient of the protection. For the protection of the grounding electrode line, the protection range is the full length of the line. According to the analysis in Section III, the threshold value should satisfy  $Z_{\text{set}} < |Z_{\text{mea}}(l, R_{\text{eq,max}}) - Z_{\text{normal}}|$ , so the upper limit of the threshold value  $Z_{\text{set,up}}$  can be determined according to the line parameters. When  $K_{\text{sen}}$  is larger than 1, the threshold value  $Z_{\text{set}}$  is selected smaller than  $Z_{\text{set,up}}$ , and the sensitivity can be ensured in the whole range theoretically. However, there can be noise interference and transformer measurement error in practical engineering. As a result,  $K_{\text{sen}}$  should not be selected too close to 1, to prevent loss of sensitivity under noise interference and error. Therefore, with reference to the value of the sensitivity coefficient in traditional AC protection,  $K_{\text{sen}}$  is selected as 1.3 in this paper, and thus, the threshold value is finally set as  $15.52\ \Omega / 1.3 = 11.94\ \Omega$ . The improved threshold

value selection is shown in Fig. 6.

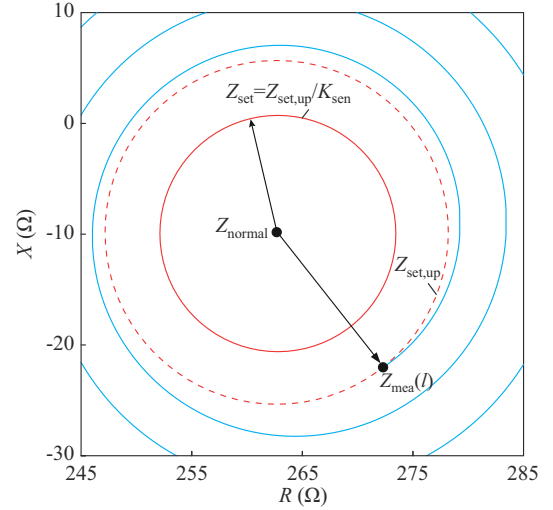


Fig. 6. Improved threshold value selection.

In practical engineering, after a grounding electrode line is built, the measured impedance during system normal operation can be easily obtained through on-site measurement. Then,  $Z_{\text{normal}}$  in the protection can be determined according to the actual measurement result. However, as analyzed above, the parameter error has a minor effect on threshold value  $Z_{\text{set}}$ . This means that  $Z_{\text{set}}$  can be completely calculated without on-site measurement.

In addition, it should be noted that, in practical engineering, only the  $13.95\ \text{kHz}$  signal is used for injection. In other words, in different existing HVDC systems, the signal frequencies are all  $13.95\ \text{kHz}$ , and there is no frequency conversion or multiple frequencies used. Therefore, the impedance characteristics for  $13.95\ \text{kHz}$  are analyzed in this paper, which is the most suitable for practical engineering needs. For different frequencies which will be probably used in the future, the calculation expressions of the measured impedance obtained in this paper (such as (5), (12), (14), (15)) and the proposed improved threshold value selection method are all suitable. If the frequency varies, just recalculate parameters according to the line structure and substitute the parameters into the corresponding expressions, and then the proper threshold value for new frequency can be obtained again. Besides, as mentioned in Section II-A, the PI control is used in the configuration of the current source and the whole structure forms negative feedback. Therefore, both the amplitude and frequency of the injected current waveform can be stabilized, and the frequency error is not discussed in this paper.

In this section, the expressions of measured impedance under fault conditions are deduced. Then, the characteristics of the measured impedance are obtained, and it can be observed that with the empirical threshold value, the protection cannot identify the fault with long fault distance and high transition resistance. As discussed in Section I, the fault with high transition resistance can cause great power loss and fire risk. Obviously, the problem should be solved, or the operation security and reliability of the HVDC system cannot be

guaranteed. Therefore, an improved threshold value selection method is proposed to ensure that the protection can detect faults with high transition resistance correctly and to guarantee the operation security and reliability of the HVDC system. In addition, in order to facilitate practical engineering applications, the line parameter error is also considered, as well as the signal frequency.

#### IV. CASE STUDIES

To verify the correctness of the theoretical analysis, different types of faults on the grounding electrode line are simulated in this section. And the performances of the impedance protection with traditional and proposed threshold value selection methods are compared, to prove the feasibility of the proposed method.

Specifically, a simulation model of an  $\pm 500$  kV HVDC system with a grounding electrode line is built on the PSCAD/EMTDC platform whose structure is shown in Fig. 1(a). The rated transmission capacity of the HVDC system is 1000 MW. For the grounding electrode line, the frequency-dependent model is used, and its structure is presented in Fig. 1(c). With the structure of the line, the values of the ground-mode propagation coefficient, the line-mode propagation coefficient, the ground-mode wave impedance, and line-mode wave impedance can be calculated as  $(1.1777 \times 10^{-5} + j3.3411 \times 10^{-4}) \text{ m}^{-1}$ ,  $(6.4798 \times 10^{-7} + j2.9331 \times 10^{-4}) \text{ m}^{-1}$ ,  $(526.73 - j18.56) \Omega$ , and  $(267.72 - j0.58) \Omega$ , respectively. The length of the grounding electrode line is 100 km, and the grounding electrode resistance is  $0.5 \Omega$ . Besides, the wave trapper is composed of a 260 nF capacitor and a 0.5 mH inductor.

##### A. Correctness of Theoretical Calculation of Measured Impedance

Firstly, the metallic double line-to-ground fault with different fault distances is simulated to verify the correctness of the theoretical analysis for measured impedance. The corresponding measured impedances and the theoretical calculated impedances are shown in Fig. 7(a). It can be concluded that all the simulation results coincide with the theoretical calculated trajectories. Furthermore, in Fig. 7(b), the single line-to-ground faults with transition resistance of  $300 \Omega$  with different fault distances are simulated, and the simulation results also coincide with the theoretical calculated trajectory. This condition indicates that the proposed method to calculate the measured impedance is correct and highly accurate, so the threshold value selection can be further developed based on the theoretical analysis.

In addition, take the method in [13] as an example, where the coupling between lines is not considered, to discuss the errors and compare it with the proposed method in this paper. With the structure of the grounding electrode line used in this paper, the measured impedance under metallic double line-to-ground fault is calculated according to (9) in [13]. In [13], the measured impedance under metallic double line-to-ground fault is an imaginary number, which varies between  $j6.0574 \times 10^6 \Omega$  and  $-j2.3603 \times 10^7 \Omega$  when the fault dis-

tance varies from 0 to 100 km. However, the actual measured impedance is shown in Fig. 7(a), which is a complex number with a spiral trajectory in the complex plane. In fact, the actual measured impedance coincides very closely with the calculated trajectory according to the proposed method in this paper, while the trajectory of the calculated measured impedance according to [13] will be a straight line along the imaginary axis, with the value between  $j6.0574 \times 10^6 \Omega$  and  $-j2.3603 \times 10^7 \Omega$ . To be more specific, the maximum value of the measured impedance modulus calculated according to the method in this paper is  $j4.7351 \times 10^3 \Omega$ . Therefore, the method in [13] not only loses all the phase information of the measured impedance, but also cannot accurately obtain the amplitude information. In contrast, the method in this paper can obtain both the amplitude and the phase precisely, which is an advantage over other methods.

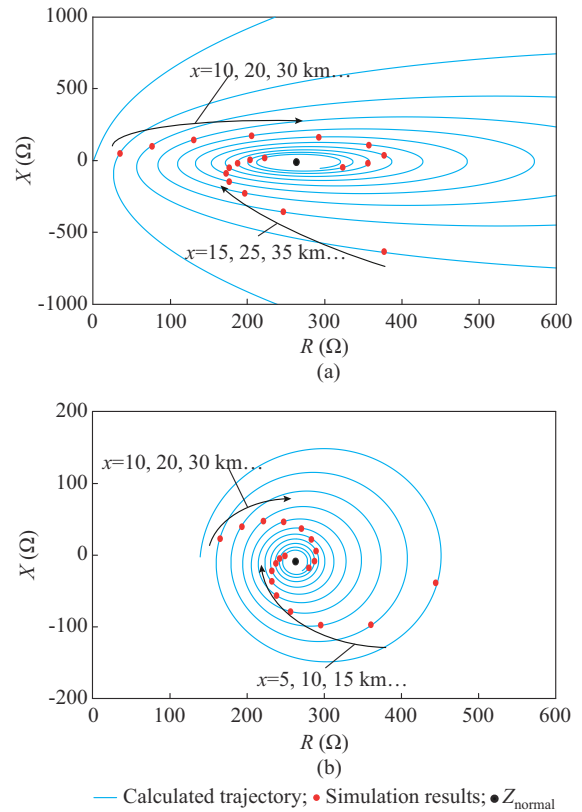


Fig. 7. Measured impedance under single and double line-to-ground faults. (a) Metallic double line-to-ground fault. (b) Single line-to-ground fault.

##### B. Performance of Impedance Protection with Traditional Threshold Value

Different types of faults are set at different positions of  $x = 10$  km and  $x = 90$  km on the grounding electrode line (at  $t = 1$  s). Then, at the station side, the waveforms of measured voltage  $\dot{U}_{in}$  are shown in Fig. 8. As the signal is injected by a current source, whose current remains constant before and after the fault, the change in measured voltage indicates the change in measured impedance.

When  $x = 10$  km, the voltage changes obviously. Thus, the protection can operate correctly regardless of the fault type.

Figure 9 shows the measured impedance after faults on the complex plane. When the metallic fault occurs, the measured impedance is outside the operation trajectory circle with traditional threshold value of  $30 \Omega$ . However, when a fault occurs at  $x=90$  km with transition resistance of  $300 \Omega$ , the voltage change is extremely small in both the amplitude and phase. Owing to the current source injection, the measured impedance also does not change obviously. The measured impedance is within the operation trajectory circle. Therefore, if the threshold value is not set properly, a maloperation will occur. The performance of the protection with the threshold values set by traditional method and proposed method is given as follows.

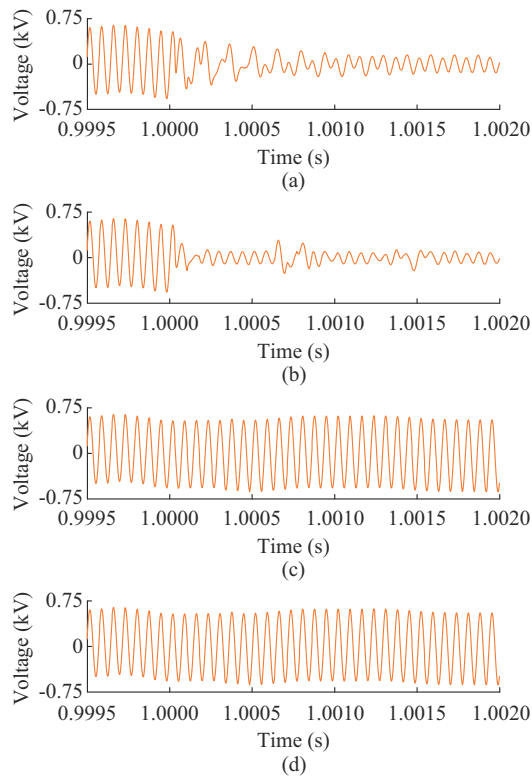


Fig. 8. Waveforms of measured voltage at station side. (a) Double line-to-ground fault when  $x=10$  km and  $R_3=0 \Omega$ . (b) Single line-to-ground fault when  $x=10$  km and  $R_3=0 \Omega$ . (c) Double line-to-ground fault when  $x=90$  km and  $R_3=300 \Omega$ . (d) Single line-to-ground fault when  $x=90$  km and  $R_3=300 \Omega$ .

It should also be pointed out that, in Fig. 8, there are some transient processes after faults and the measured impedance changes correspondingly. However, the transient processes represent the traveling waves caused by faults, and the traveling wave decays rapidly, which means the transient process ends. The fault correspondingly enters the steady-state stage. Generally speaking, in the bipolar mode of HVDC system, the fault on the ground electrode line does not influence the normal operation of the system immediately, the time delay of the ground electrode line protections can be longer than that of AC or DC protection. Besides, in most situations, only an alarm signal is sent out or some actions are taken on the system operation, while there is no need to trip the breaker. In fact, the time delay of the ELIS-

based protection is 10 s, and after 10 s, an alarm signal is sent out. In the ELIS-based protection, the main focus is on the impedance characteristics in steady state. As shown in Fig. 8, the traveling wave decays in 2 ms, which is very short compared with 10 s. So, the transient processes after faults are not taken into consideration, and the measured impedance during faults does not influence the correct action of the protection.

### C. Performance of Impedance Protection with Threshold Value Selected by Proposed Method

According to the proposed method and system parameters, the threshold value of the impedance protection can be selected as  $11.94 \Omega$  and  $K_{\text{sen}}=1.3$ . Table I shows the operation results of the impedance protection with the threshold value  $11.94 \Omega$ . Meanwhile, the operation results of the protection with traditional threshold value, i. e.,  $30 \Omega$ , are also displayed for comparison in Fig. 9. With the proposed threshold value, the protection can operate correctly under different types of faults, even with long distance and large resistance. This condition means that the protection operation sensitivity with the selected threshold value is improved significantly.

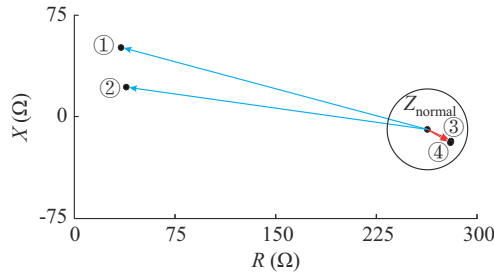
In addition, the comparison between the proposed method in this paper and the method in [13] is also given in Table I. In [13], a frequency selection criterion to eliminate the operation dead zone is proposed, and  $13.853$  kHz is selected as the optimum frequency instead of threshold value selection. According to [13], the dead zone exists when the grounding electrode line length is an integer multiple of the half-wavelength of the injected current. Because the wavelength of the injected current under  $13.853$  kHz is  $20.36$  km and the grounding electrode line length is  $100$  km, there is no dead zone for the method in [13]. However, according to the simulation results, simply optimizing the frequency does not solve the dead zone problem. The dead zone still exists when the transition resistance is  $300 \Omega$  and the fault distance is greater than  $75$  km, regardless of the fault type. That is to say, compared with the traditional method, the method in [13] has little improvement effect, while the proposed method in this paper can eliminate the dead zone and the protection operation sensitivity improvement is furtherly confirmed.

In this section, simulation case studies are used and the conclusions in the above sections are proved. The correctness of theoretical calculation of measured impedance is first verified, which is the basis for subsequent analysis. Then, the performance of the impedance protection with traditional threshold value is presented and discussed, which has a limitation in detecting faults with high transition resistance. Therefore, the performance of the impedance protection with threshold value selected by the proposed method is also presented and discussed. The simulation results show that the proposed method in this paper can eliminate the dead zone and the improve protection operation sensitivity greatly. In addition, the comparison between the proposed method and the method in [13] is also given, which further highlights the value of the method proposed in this paper.

TABLE I  
PROTECTION OPERATION RESULTS

Fault distance (km)	Transition resistance ( $\Omega$ )	Protection operation results under double line-to-ground fault			Protection operation results under single line-to-ground fault		
		Traditional threshold value	Proposed threshold value	Method in [13]	Traditional threshold value	Proposed threshold value	Method in [13]
25	0	+	+	+	+	+	+
	300	+	+	+	+	+	+
50	0	+	+	+	+	+	+
	300	+	+	+	+	+	+
75	0	+	+	+	+	+	+
	300	-	+	-	-	+	-
80	0	+	+	+	+	+	+
	300	-	+	-	-	+	-
85	0	+	+	+	+	+	+
	300	-	+	-	-	+	-
90	0	+	+	+	+	+	+
	300	-	+	-	-	+	-
95	0	+	+	+	+	+	+
	300	-	+	-	-	+	-
99	0	+	+	+	+	+	+
	300	-	+	-	-	+	-

Note: + indicates that the protection operation result is correct, while - shows that the protection fails to operate.



- ① Double line-to-ground fault,  $x=10$  km,  $R_3=0$   $\Omega$ ,  $|Z_{mea}-Z_{normal}|=236.43$   $\Omega$
- ② Single line-to-ground fault,  $x=10$  km,  $R_3=0$   $\Omega$ ,  $|Z_{mea}-Z_{normal}|=226.70$   $\Omega$
- ③ Single line-to-ground fault,  $x=90$  km,  $R_3=300$   $\Omega$ ,  $|Z_{mea}-Z_{normal}|=19.66$   $\Omega$
- ④ Double line-to-ground fault,  $x=90$  km,  $R_3=300$   $\Omega$ ,  $|Z_{mea}-Z_{normal}|=19.80$   $\Omega$

Fig. 9. Performance of impedance protection with traditional threshold value.

## V. CONCLUSION

In the HVDC transmission system, the ELIS-based protection has good prospects for application in the grounding electrode line. However, due to the rough selection of the threshold value, a serious accident occurs because there is still a lack of reasonable improvements in the ELIS-based protection. In this study, the accurate calculation expressions of measured impedance of the ELIS-based protection in various conditions are deduced, based on the electromagnetic wave theory and decoupling concept. Then, the characteristics of the measured impedances are discussed in detail. The results show that the ELIS-based protection with traditional threshold value has a large operation dead zone, especially under faults with high transition resistances. Therefore, the improved method to calculate the threshold value has been proposed considering the line parameter error. The simulation re-

sults verify that, with the selected threshold value, the ELIS-based protection can operate with high sensitivity under all types of faults even with large transition resistances. Thus, the operation security and reliability of the HVDC system can be improved. In addition, the characteristics analysis of the measured impedance is also of great significance in applications such as the verification of ELIS-based protection performance in existing or new HVDC projects and the research of fault location method.

## REFERENCES

- [1] T. Li, Y. Li, and X. Chen, "Fault diagnosis with wavelet packet transform and principal component analysis for multi-terminal hybrid HVDC network," *Journal of Modern Power Systems and Clean Energy*, vol. 9, no. 6, pp. 1312-1326, Nov. 2021.
- [2] T. Wu, Y. Zheng, Q. Liu *et al.*, "Continuous commutation failure suppression method based on self-adaptive auto-disturbance rejection proportional-integral controller for HVDC transmission system," *Journal of Modern Power Systems and Clean Energy*, vol. 8, no. 6, pp. 1178-1187, Nov. 2020.
- [3] T. An, C. Han, Y. Wu *et al.*, "HVDC grid test models for different application scenarios and load flow studies," *Journal of Modern Power Systems and Clean Energy*, vol. 5, no. 2, pp. 262-274, Mar. 2017.
- [4] M. Muniappan, "A comprehensive review of DC fault protection methods in HVDC transmission systems," *Protection and Control of Modern Power Systems*, vol. 6, no. 1, pp. 1-20, Jan. 2021.
- [5] Y. Liu, B. Li, B. Li *et al.*, "Research on power flow calculation and optimization method of real bipolar VSC-HVDC grid under asymmetrical mode," in *Proceedings of 2018 IEEE PES General Meeting*, Portland, USA, Aug. 2018, pp. 1-5.
- [6] Z. Wang, Y. Zhang, Z. Ren *et al.*, "Modeling of anisotropic magnetostriction under DC bias based on an optimized BP neural network," *IEEE Transactions on Magnetics*, vol. 56, no. 3, pp. 1-4, Mar. 2020.
- [7] C. Pan, S. Yi, H. Su *et al.*, "Excitation-vibration harmonic response research of transformer in DC biasing operation," *IET Electric Power Applications*, vol. 13, no. 3, pp. 410-417, Mar. 2019.
- [8] J. He, Z. Yu, R. Zeng *et al.*, "Vibration and audible noise characteristics of AC transformer caused by HVDC system under monopole operation," *IEEE Transactions on Power Delivery*, vol. 27, no. 4, pp. 1835-1842, Oct. 2012.

- [9] Z. Yu, L. Liu, Z. Wang *et al.*, "Evaluation of the interference effects of HVDC grounding current on a buried pipeline," *IEEE Transactions on Applied Superconductivity*, vol. 29, no. 2, pp. 1-5, Mar. 2019.
- [10] C. A. Charalambous, A. Dimitriou, I. Gonos *et al.*, "Modelling and assessment of short-term electromagnetic interference on a railway system from pole-to-ground faults on HVDC cable networks," in *Proceedings of 2019 IEEE International Conference on Environment and Electrical Engineering and 2019 IEEE Industrial and Commercial Power Systems Europe (EEEIC/I&CPS Europe)*, Genova, Italy, Aug. 2019, pp. 1-6.
- [11] L. Yang, W. Sima, and Q. Yang, "Simulation analysis on lightning accident of  $\pm 500$  kV DC transmission line based on ATP-EMTP," in *Proceedings of 2008 International Conference on High Voltage Engineering and Application*, Chongqing, China, Apr. 2009, pp. 317-320.
- [12] G. Asplund, "Electrode line protection," U.S. Patent 5117323, May 26, 1992.
- [13] Y. Teng, Z. Zhang, and X. Li, "Improved approach to high-frequency current injection-based protection for grounding electrode line in high-voltage direct current system," *IEEE Transactions on Industry Applications*, vol. 56, no. 3, pp. 2409-2417, May-Jun. 2020.
- [14] Y. Teng, X. Li, Q. Huang *et al.*, "A novel high-frequency voltage standing-wave ratio-based grounding electrode line fault supervision in ultra-high voltage DC transmission systems," *Energies*, vol. 10, pp. 1-17, Mar. 2017.
- [15] S. Li, X. Li, Y. Teng *et al.*, "A novel protection method for grounding electrode line of UHVDC based on injection current," in *Proceedings of 2020 IEEE/IAS Industrial and Commercial Power System Asia (I&CPS Asia)*, Weihai, China, Sept. 2020, pp. 910-915.
- [16] Y. Zhuang, Y. Teng, X. Li *et al.*, "A new method for HVDC grounding electrode line protection based on multi-band voltage amplitude integration," in *Proceedings of 2019 IEEE Innovative Smart Grid Technologies - Asia (ISGT Asia)*, Chengdu, China, Oct. 2019, pp. 2223-2227.
- [17] B. Li, Q. Sun, J. He *et al.*, "An improved protection scheme of the ground electrode line based on two frequency components injection," *International Journal of Electrical Power & Energy Systems*, vol. 129, pp. 106901-106914, Jul. 2021.
- [18] X. Li, Y. Teng, X. Song *et al.*, "Performance analysis of the ELIS system for UHVDC grounding electrode line under line break faults," in *Proceedings of 2019 IEEE Innovative Smart Grid Technologies - Asia (ISGT Asia)*, Chengdu, China, May 2019, pp. 2173-2177.
- [19] M. V. der Linde, "Fire risk mitigation in the overhead electricity distribution network," in *Proceedings of 2019 29th Australasian Universities Power Engineering Conference (AUPEC)*, Nadi, Fiji, Nov. 2019, pp. 1-6.
- [20] Y. Teng, Z. Zhang, and X. Li, "An improved grounding electrode line protection for high-voltage direct current system based on high frequency signal injection," in *Proceedings of 2019 IEEE Industry Applications Society Annual Meeting*, Baltimore, USA, Sept. 2019, pp. 1-7.
- [21] A. S. Al-Fuhaid and M. M. Saied, "A method for the computation of fault transients in transmission lines," *IEEE Transactions on Power Delivery*, vol. 3, no. 1, pp. 288-297, Jan. 1988.
- [22] H. Xu, R. Zhang, X. Li *et al.*, "Fault tripping criteria in stability control device adapting to half-wavelength AC transmission line," *IEEE Transactions on Power Delivery*, vol. 34, no. 4, pp. 1619-1625, Aug. 2019.
- [23] N. G. Hingorani, "Transient overvoltage on a bipolar HVDC overhead line caused by DC line faults," *IEEE Transactions on Power Apparatus and Systems*, vol. PAS-89, no. 4, pp. 592-610, Apr. 1970.
- [24] Y. Zhang, N. Tai, and B. Xu, "Fault analysis and traveling-wave protection scheme for bipolar HVDC lines," *IEEE Transactions on Power Delivery*, vol. 27, no. 3, pp. 1583-1591, Jul. 2012.
- [25] A. Budner, "Introduction of frequency-dependent line parameters into an electromagnetic transients program," *IEEE Transactions on Power Apparatus and Systems*, vol. PAS-89, no. 1, pp. 88-97, Jan. 1970.

**Qiang Sun** received the B.Sc. degree in electrical engineering from Xi'an Jiaotong University, Xi'an, China, in 2018, and the M.Sc degree in electrical engineering from Tianjin University, Tianjin, China, in 2021. His research interests include protection and control of HVDC system and flexible DC grid.

**Bin Li** received the B.Sc, M.Sc, and Ph.D. degrees in electrical engineering from Tianjin University, Tianjin, China, in 1999, 2002, and 2005, respectively. He was an Academic Visitor of the University of Manchester, Manchester, U.K., in 2006. He worked in the design and application of protection relays in AREVA Company U.K. from 2008 to 2009. Currently, he is a Professor with the School of Electrical Engineering and Its Automation, Tianjin University. His main research interests include protection and control of power system.

**Jiawei He** received the B.Sc., M.Sc., and Ph.D. degrees in electrical engineering from Tianjin University, Tianjin, China, in 2014, 2017, and 2021, respectively. He is currently an Associate Researcher Fellow with Tianjin University. His research interests include protection and control of flexible DC grid, AC-DC hybrid power system, and renewable power generation.

**Ye Li** received the B.Sc., M.Sc., and Ph.D. degrees in electrical engineering from Tianjin University, Tianjin, China, in 2015, 2017, and 2021, respectively. She is currently a Lecturer with the Hebei University of Technology, Tianjin, China. Her research interests include protection and control of DC grid and AC-DC distribution network.